TWELFTH EUROPEAN ROTORCRAFT FORUM

Paper No. 32

UNSTEADY SEPARATION CHARACTERISTICS OF AIRFOILS OPERATING UNDER DYNAMIC STALL CONDITIONS

W. Geißler
DFVLR Institute of Aeroelasticity, Göttingen, F.R. Germany

L.W. Carr
US Army Aeromechanics Laboratory, NASA-Ames Research Center
Moffett Field, California, USA

T. Cebeci
Center for Aerodynamic Research, Cal. State University,
Long Beach, California, USA

September 22 - 25, 1986

Garmisch-Partenkirchen
Federal Republic of Germany

Deutsche Gesellschaft für Luft- und Raumfahrt e.V. (DGLR)
Godesberger Allee 70, D-5300 Bonn 2, F.R.G.

UNSTEADY SEPARATION CHARACTERISTICS OF AIRFOILS OPERATING UNDER DYNAMIC STALL CONDITIONS

by

Wolfgang Geißler,* Lawrence W. Carr,** Tuncer Cebeci***

Abstract

Within the scope of a joint effort between DFVLR, NASA-Ames and Cal. State University Long Beach, represented by the authors, unsteady viscous/inviscid interaction phenomena have been investigated on airfoils operating under dynamic stall conditions. It is well known from experiments that, in the upstroke region of a sinusoidally oscillating airfoil, the flow remains attached up to incidences considerably larger than the static stall angle. Reversed flow areas develop close to the airfoil surface without boundary layer separation. These complicated flow phenomena are investigated in the present study on the basis of coupling procedures between a time-dependent inviscid panel method and 2-d unsteady boundary layer codes. Two strategies are pursued:

1. Coupling of inviscid panel method with boundary layer code — direct mode.
2. Strong coupling of inviscid panel method with boundary layer code — inverse mode.

The main features of the unsteady time-marching panel method and boundary layer codes are discussed. Emphasis is placed on the investigation of numerical stability and the phenomenon of unsteady separation. Future steps of the ongoing cooperation are outlined.

1. Introduction

The dynamic stall problem is closely related to helicopter aerodynamics. On the retreating blade of a helicopter in forward flight, the flow may separate and reattach, leading to very complicated time-dependent flow phenomena. In the present study this problem is simplified in the usual way by representing the rotating blade by a nonrotating characteristic airfoil section undergoing pitching oscillations about the quarter-chord axis. Extensive windtunnel experiments [1] have shown that the following list of parameters is of the highest importance for dynamic stall characteristics:

---

* DFVLR Institute of Aeroelasticity, Göttingen, West Germany
** US Army Aeromechanics Laboratory, NASA-Ames Research Center, Moffett Field, California, USA
*** Center for Aerodynamic Research, Cal. State Univ., Long Beach, California, USA

airfoil shape	Mach number
Reynolds number	reduced frequency
mean angle, amplitude	type of motion
3-d effects	tunnel effects

A calculation procedure should have the capability to take most of these parameters into account. This has been verified in the present methods with the exceptions of 3-d and tunnel effects.

Fig.1 shows measured lift and pitching moment distributions as functions of incidence together with the related flow events [2]. The lift curve shows a considerable extension beyond the static stall angle during upstroke. In this regime the boundary layer on the upper surface still remains attached. Hot film measurements and flow visualizations have shown however that, at these incidences, the flow inside the boundary layer is partially reversed. This reversed flow area is located adjacent to the wall and may spread over most of the upper surface. Lift and moment curves show the characteristic hysteresis loops.

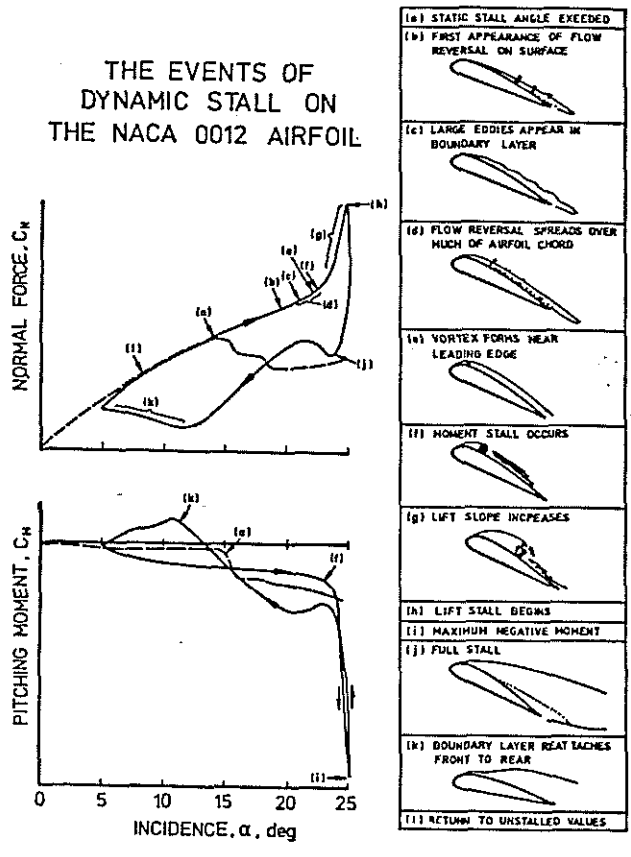

Fig.1

In the present study the upstroke region will be investigated on the basis of coupling procedures between an unsteady inviscid panel method and time-dependent boundary layer codes. Recent investigations with unsteady finite difference boundary layer procedures [3,4,5] have shown that calculations within reversed flow areas are possible. In the following discussion the limits of these methods due to numerical stability (CFL condition) as well as due to unsteady separation (MRS criterion) will be outlined. Two different strategies of coupling procedures between inviscid and viscous methods will be applied:

- weak coupling, boundary layer calculation in the direct mode
- strong coupling, boundary layer calculation in the inverse mode.

Some typical results of these calculations will be given. Further steps are necessary and planned in the future to improve the various codes.

2. Unsteady Inviscid Panel Method

Fig.2a shows the nomenclature of profile and wake for the unsteady panel method. Both profiles and wake surfaces are subdivided into panels, each of which is represented by a constant source and vorticity distribution. The vorticity distribution is extended into the unsteady wake. The wake geometry is simplified by a straight line.

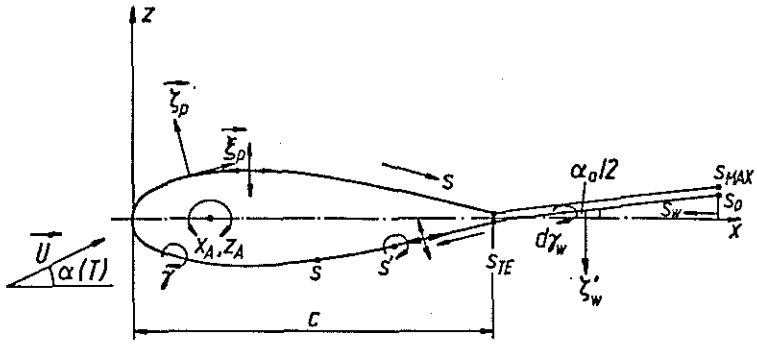

s : Surface coordinate (Control point)
s' : Surface coordinate (Integration variable)
$\vec{\xi}$: Unit tangential vector (in s-direction)
$\vec{\zeta}$: Unit normal vector (outer normal direction)

Fig.2a Nomenclature

The incidence variation

$$(1)\quad \alpha(T) = \alpha_0 + \alpha_1 \sin\omega^* T$$

with $T = \frac{t \cdot U_\infty}{c}$; $\omega^* = \frac{\omega \cdot c}{U_\infty}$

is subdivided into time steps. For each time step the kinematic flow condition (zero normal velocity on the profile surface) is fulfilled and the strengths of the source and vorticity distributions are determined by solving a linear system of equations. The resulting relative velocity vector used in the boundary layer codes as an outer boundary condition is obtained by

$$(2)\quad \vec{w} = \vec{V}_{kin} + \vec{v}_q + \vec{v}_\gamma \equiv U_e(x,T)$$

with $\vec{V}_{kin}$ as the prescribed kinematic velocity and $\vec{v}_q$ and $\vec{v}_\gamma$ as the induced velocities of the source and vorticity system.

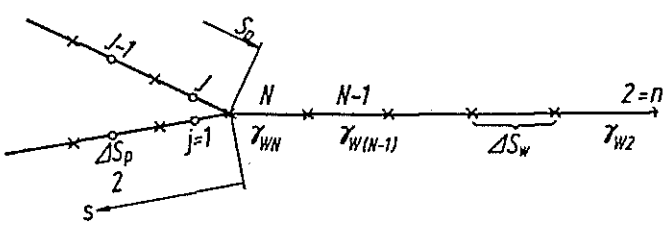

$$\Delta S_w \equiv \Delta T = \Delta\bar{T} \cdot \frac{2\pi}{\omega^*}$$

$$\gamma_w = -\Delta\gamma_p \cdot \frac{S_p}{\Delta T} = -\Delta\gamma_p \cdot \frac{S_p \cdot \omega^*}{\Delta\bar{T} \cdot 2\pi}$$

ΔS_w : Length of Wake Element
ΔS_p : Length of Profile Panel
$\Delta\gamma_p$: Change of Profile Vorticity during Time step ΔT

Fig.2b Relation between profile and wake vorticity

The unsteady Bernoulli equation determines the pressure coefficient

$$(3)\quad C_p(T) = -2\frac{\partial\varphi}{\partial T} + \vec{V}_{kin} \cdot \vec{V}_{kin} - \vec{w} \cdot \vec{w}$$

with $\varphi(T)$ as the velocity potential.

By means of the unsteady Kutta condition

$$(4)\quad \lim_{s \to s_{T.E.}} \left(C_{p_u}(T) - C_{p_\ell}(T) \right) = 0$$

(s ≡ surface coordinate)

the vorticity loading of the wake element leaving the trailing edge at time T is specified. Fig.2b describes the relationship between profile and wake vorticity. After each time step a new

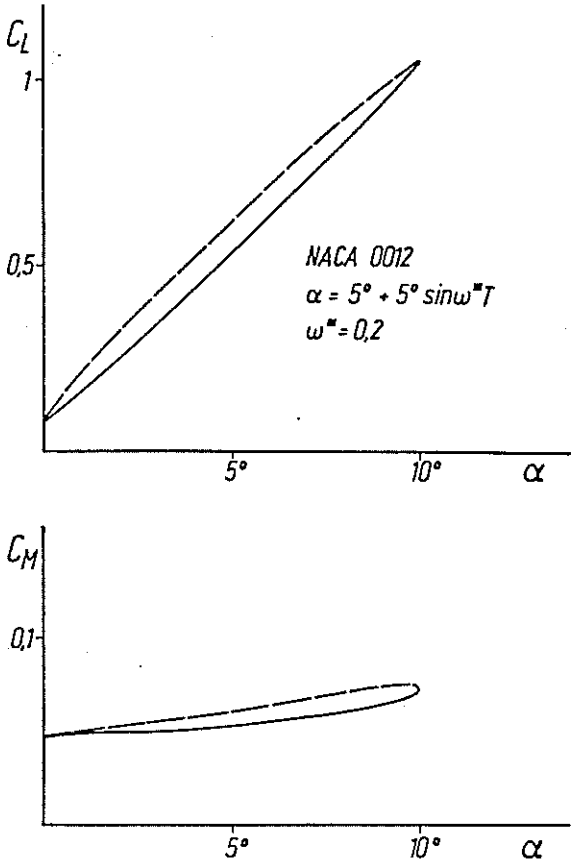

wake element is shed at the trailing edge which then moves downstream with U_∞.

A more detailed description of the method is given in [6]. As a typical result of the unsteady panel method, lift and moment distributions for three different reduced frequencies are presented in Figs.3a-3c for the NACA 0012 airfoil. Due to unsteady wake effects, hysteresis loops develop even in the present inviscid case: for small values of ω^* (Fig.3a) the lift loop is traversed in counterclockwise direction. For higher values of ω^* (Fig.3c) this trend is reversed. For an intermediate value of ω^* (Fig.3b), a hysteresis loop for the lift has disappeared entirely. The influence of ω^* on the pitching moment is minor.

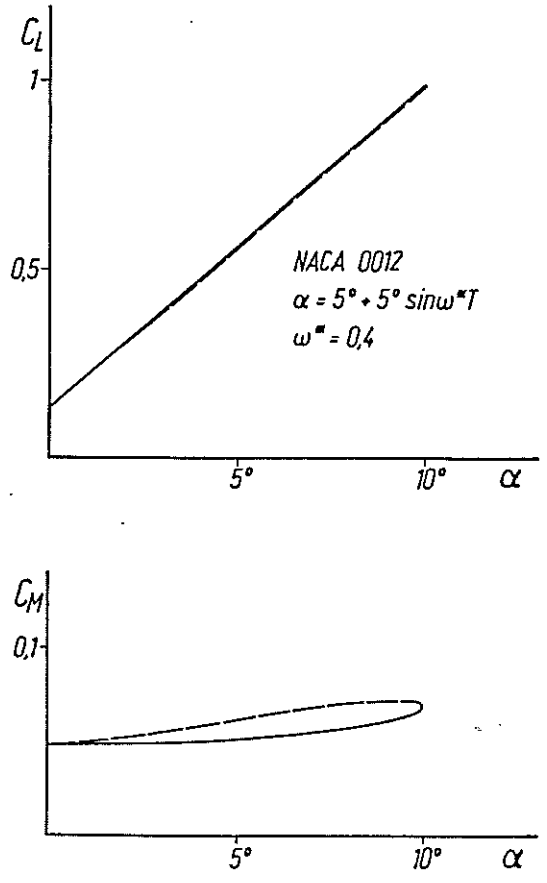

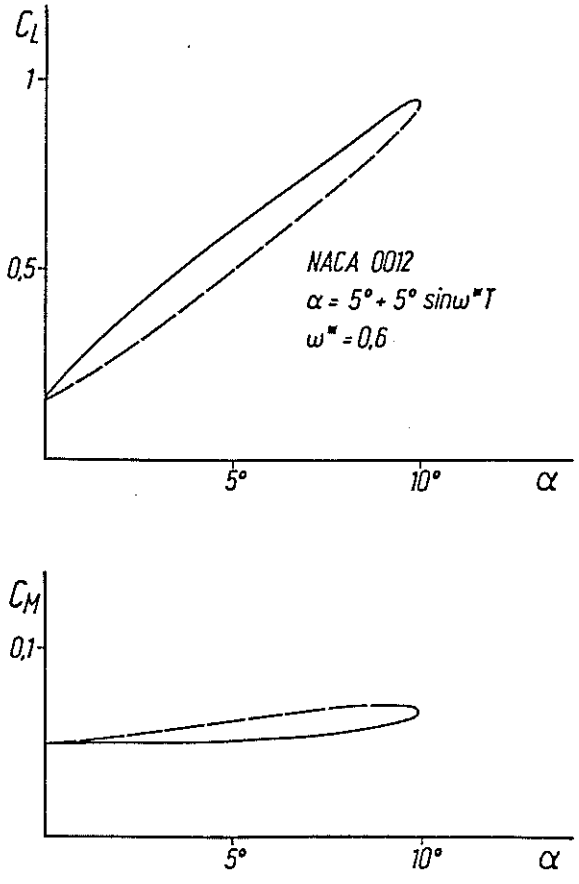

Fig.3a,b,c Unsteady inviscid lift and moment distributions

3. Unsteady (Laminar/Turbulent) Boundary Layer: Direct Mode (Geißler)

3.1 Boundary Layer Calculation Procedure

In addition to the external inviscid velocity distribution $U_e(X,T)$, corresponding initial conditions are necessary to start the boundary layer calculation. Fig.4 shows as a result of the inviscid method that the front stagnation point is moving. To start the boundary layer calculation at the stagnation point for all time steps, the unsteady boundary layer equations are expressed in a stagnation-point-fixed frame of reference [5] with the coordinate

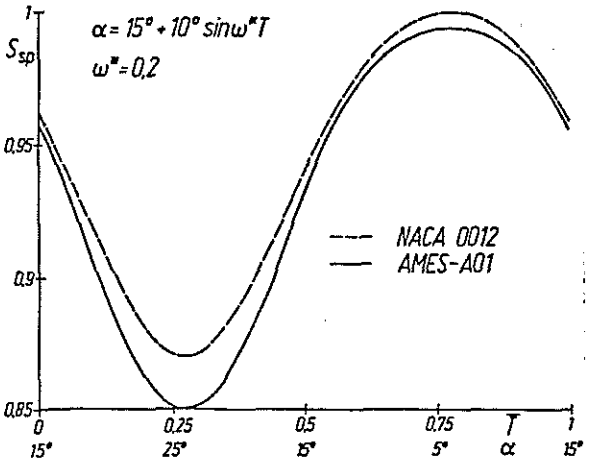

Fig.4 Displacement of stagnation point

$$(5)\quad x_{1_{u,\ell}} = \pm\left(s - s_{SP}(T)\right)$$

(s_{SP} ≡ time-dependent location of the stagnation point),

with ± referring to the upper/lower surface, respectively.

The kinematic velocity of the stagnation point is then

$$(6)\quad U_{1_{kin}} = \frac{\partial x_1}{\partial T} \ .$$

In the new system the unsteady boundary layer equations yield

$$(7)\quad \frac{\partial u_1}{\partial x_1} + \frac{\partial \bar{v}_1}{\partial \eta_1} = 0$$

$$(8)\quad \frac{\partial u_1}{\partial T} + u_1 \frac{\partial u_1}{\partial x_1} + \bar{v}_1 \frac{\partial u_1}{\partial \eta_1} = \frac{\partial U_1}{\partial T} + U_1 \frac{\partial U_1}{\partial x_1} + \frac{\partial}{\partial \eta_1}\left[\left(1 + \frac{\varepsilon_1}{\nu}\right)\frac{\partial u_1}{\partial \eta_1}\right]$$

with $\bar{v}_1 = v_1 \sqrt{Re}$; $\eta_1 = y_1 \sqrt{Re}$

and the boundary conditions

$$(9)\quad \begin{aligned} \eta_1 &= 0\ , & u_1 &= U_{1_{kin}}\ , & \bar{v}_1 &= 0\ , \\ \eta_1 &\to \infty\ , & u_1 &= U_1 + U_{1_{kin}}\ . \end{aligned}$$

For the turbulent boundary layer calculations the algebraic eddy viscosity formulation (ε_1 in Eq.(8)) by Cebeci/Smith [7] has been used. In the present investigation the transition point is fixed directly behind the (moving) stagnation point. For the boundary layer calculations in the direct mode a finite difference grid of the Crank-Nicolson type is used. Fig.5 shows as a typical result contour lines of vorticity (γ) and velocity (u) inside the boundary layer along the profile upper surface at a specific instant of nondimensional time

$$(10)\quad \bar{T} = \frac{T \cdot \omega^*}{2\pi} = 1.15$$

corresponding to the instantaneous incidence $\alpha = 19.85°\uparrow$.

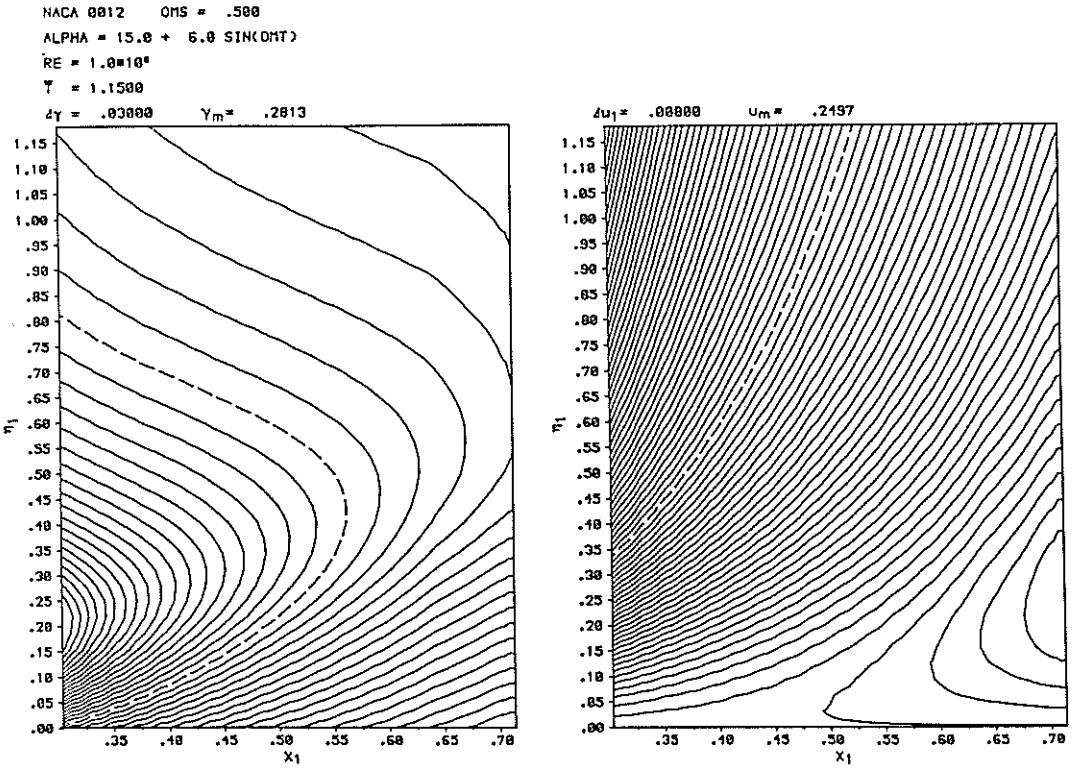

Fig.5 Contour lines of equal vorticity γ (left) and equal velocity u (right)

The calculation came to a breakdown at the right-hand margins of the figures at about $x_1 = 0.71$. This breakdown occurred due to the violation of the numerical stability condition described in the following section.

3.2 Stability Considerations

As long as the flow inside the boundary layer is non-reversed the Crank-Nicolson finite difference scheme applied for the present 2-d unsteady boundary layer equations is unconditionally stable. It is shown in Fig.6 however that stability limits exist in regions where the flow is reversed. If the characteristics of the points 1, 2, 3 where the boundary layer quantities are known are bent backwards such that no information can reach the midpoint of the difference molecule,

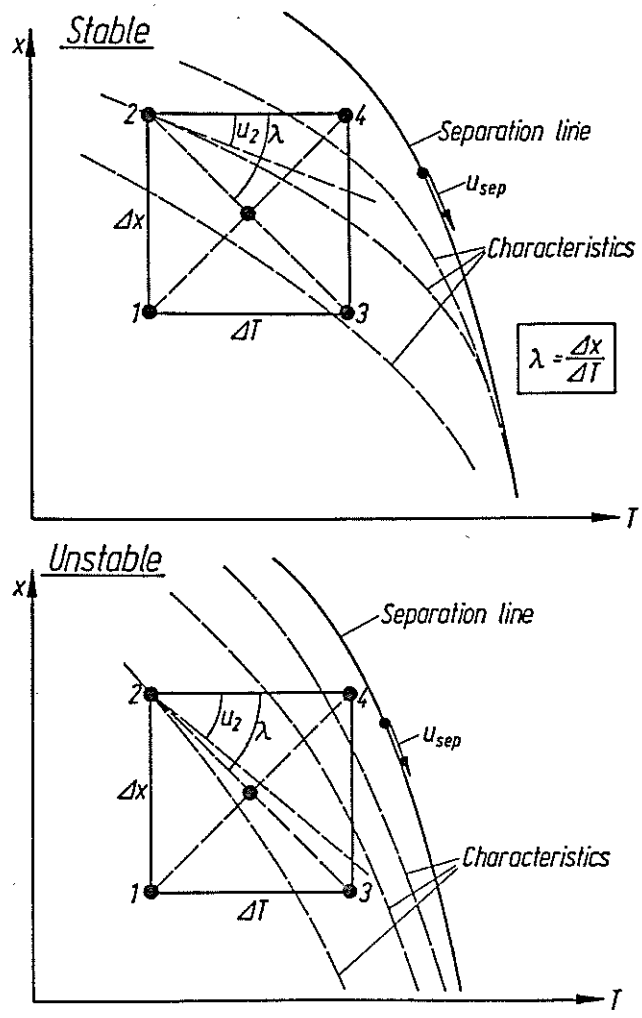

Fig.6 Stability bounds of central difference scheme

the calculation breaks down (violation of CFL condition). It is obvious that the mesh size ratio $\Delta x/\Delta T$ is the limiting value. To exceed the stability bounds the time step ΔT has to be reduced inside reversed flow areas.

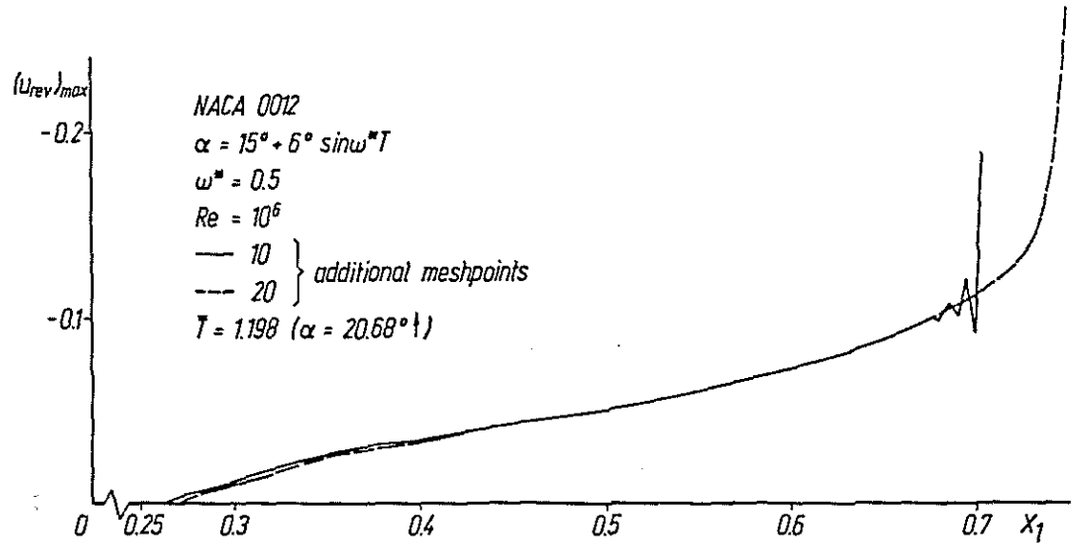

Fig.7 Maximum reversed flow velocity: investigation of the CFL condition

Fig.7 shows maximum reversed flow velocities inside the boundary layer for two different numbers of sub-time steps (original time step: $\Delta\bar{T} = 0.01$). Ten sub-time steps are not sufficient. The boundary layer calculation breaks down after a few oscillations. With twenty sub-time steps, however, a smooth increase of $(u)_{rev}$ is achieved.

3.3 Unsteady Separation

If the numerical stability bound has been removed due to a corresponding reduction of the time step, the calculation may run into a limit which must be interpreted as unsteady separation. Fig.8 shows the well-known steady separation criterion and the more complicated unsteady MRS (Moore, Rott and Sears) criterion. In the unsteady case, separation is obtained at the position of zero shear stress off the wall when the maximum reversed flow velocity at this position reaches the separation velocity. The MRS criterion cannot be checked in a simple manner during the ongoing calculation due to the unknown separation velocity.

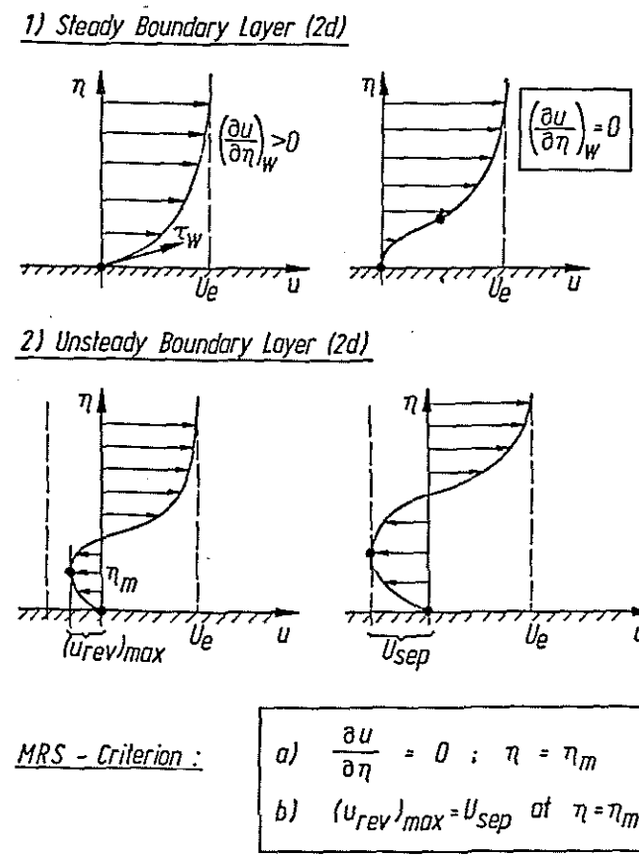

Fig.8 Separation criteria

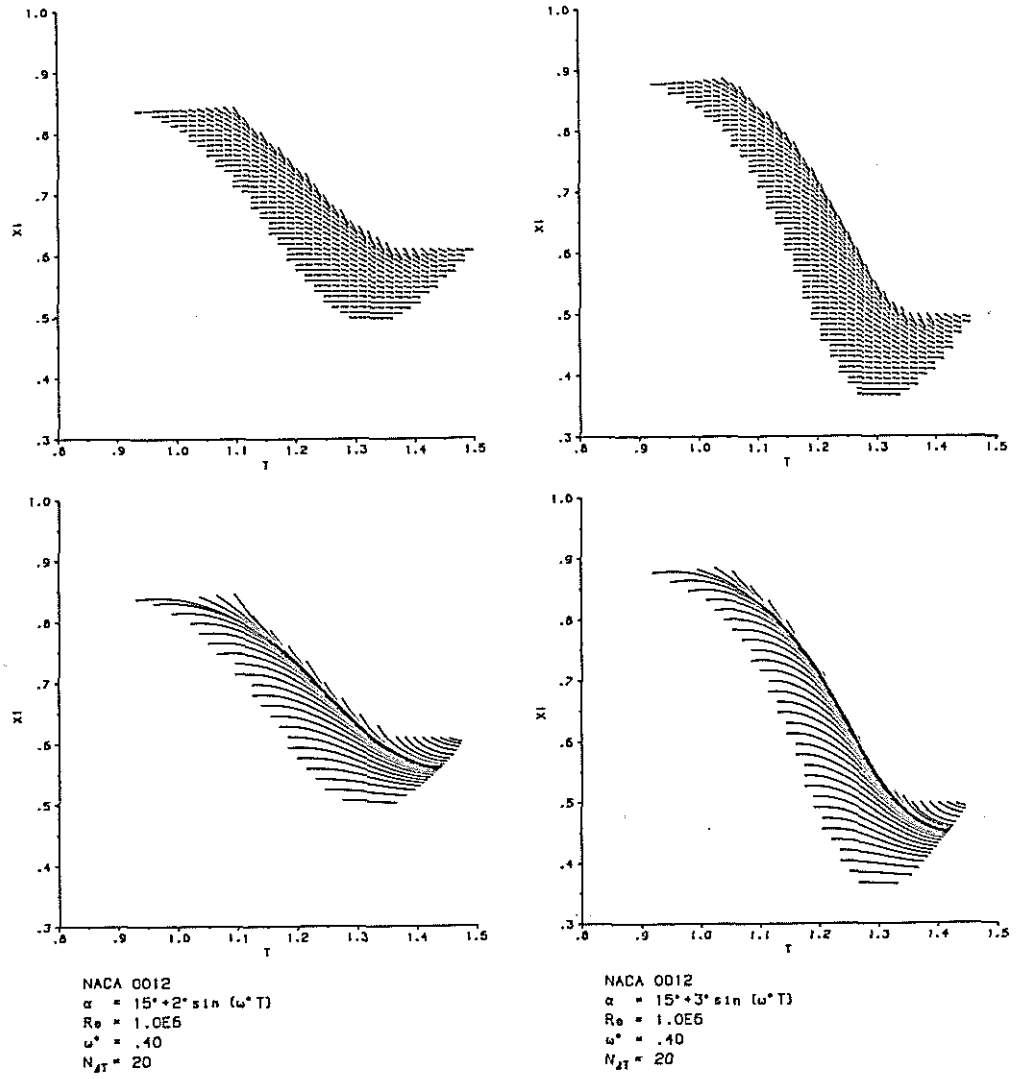

Fig.9 Reversed velocity vectors and integral curves (direct mode)

Fig.9 is an attempt to explain the MRS criterion by means of the numerical results of the maximum reversed flow velocities inside the boundary layer. The upper plots show vectors of the maximum reversed flow velocities for two different amplitudes of oscillation. The lower plots display the corresponding integral curves. These integral curves merge from both sides into one line forming an envelope which is identified as the unsteady separation line. The tangents of these lines correspond to the unsteady separation velocity. Similar behavior has already been observed in 3-d steady boundary layer calculations [8] for the integrated wall shear stress vectors.

Fig.10 displays a comparison of calculated reversed flow areas with experimental data [1] for the deep dynamic stall regime. Reattachment is approximated by the lines $\tau_W = 0$. For the higher Re-numbers the correspondence between the calculations and the experimental data is quite sufficient. Deviations occur for the low Re-number case where the assumption of a fixed transition point is no longer valid.

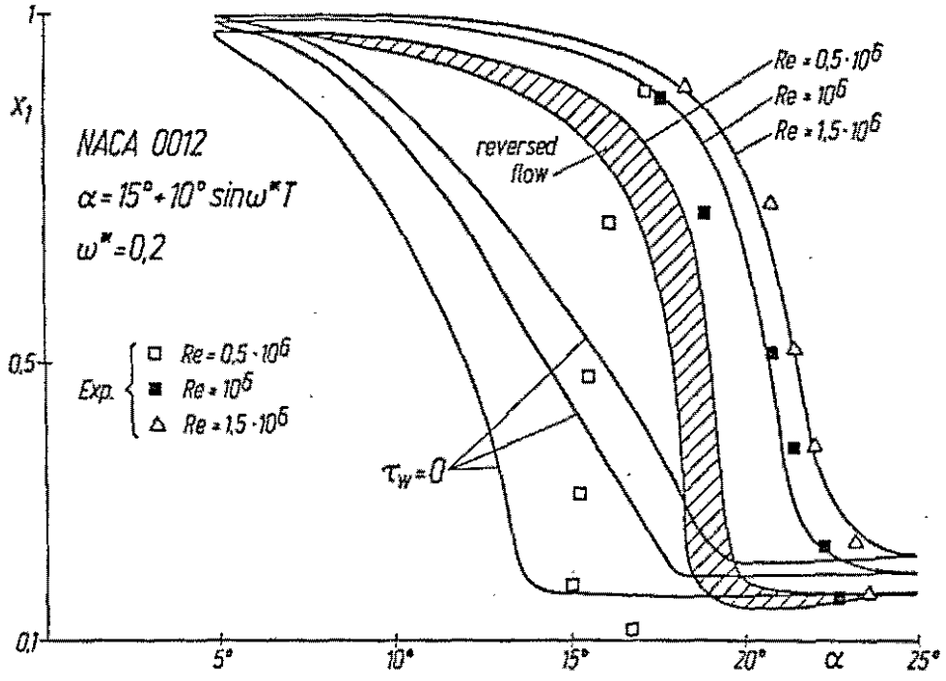

Fig.10 Separation and reattachment loops: deep dynamic stall conditions

Finally, Fig.11 shows how the results of the boundary layer calculation may be used for a modified panel method to take the location as well as the speed of unsteady separation into account. A corresponding modification of the unsteady Kutta condition for two vortical wakes has been discussed by Sears [9]. The introduction of two separating wakes in the unsteady panel method is straightforward.

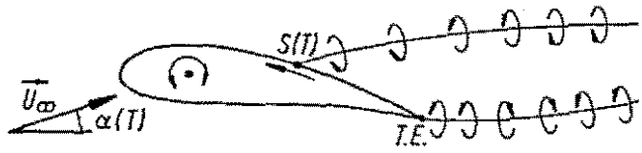

Change of Airfoil Circulation

$$-\frac{d\Gamma}{dT} = \left[\frac{1}{2}U_e^2 - U_{sep} \cdot U_e\right]_{T.E.}^{S(T)}$$

Fig.11 Modification of unsteady panel method

4. Unsteady (Laminar/Turbulent) Boundary Layer: Inverse Mode (Cebeci/Carr)

4.1 Boundary Layer Calculation Procedure

Unsteady boundary layer calculations extending into the reversed flow area for some model flows have been presented in [3] with the application of Keller's box method. Ref.[10] describes an inverse procedure for steady separating flows over profiles. A combination of these two methods has been developed. The velocity distribution obtained from the unsteady panel method presented in Section 2 serves again as the outer boundary condition.

To overcome the problem of the oscillating stagnation point the boundary layer calculation now starts from the instantaneous positions of the stagnation point on a quasi-steady basis until a prescribed position is reached, where the unsteady inverse calculation starts downstream. The unsteady boundary layer equations, Eqs.(7),(8), remain unchanged except that the stagnation-point-fixed coordinate x_1 is replaced by the profile-fixed coordinate x. The boundary conditions (Eq.(9)) are simply changed by replacing $U_{1_{kin}}$ with zero.

The calculation is now allowed to work in the inverse mode. The external velocity

$$(11) \qquad U_{ev}(x,T) = U_e(x,T) + \delta U_e(x,T)$$

with

$$(12) \qquad \delta U_e(x,T) = \frac{1}{\pi} \int_{x_a}^{x_b} \frac{d}{dx} (U_e \, \delta^*) \, \frac{dx'}{x-x'}$$

is modified by means of the blowing velocity

$$(13) \qquad v_B = \frac{d}{dx} (U_e \, \delta^*) \, .$$

Eq.(12) is the Hilbert Integral representation [10], which takes the upstream (x_a) *and* downstream (x_b) displacement effects of the boundary layer at the present position x into account. The calculation is done by several sweeps along the profile surface where the downstream displacement values are taken from the previous sweep. This sweep process is performed for each time step.

The standard box method is applied in regions where the flow is directed downstream. The zigzag scheme is used in regions of reversed flow inside the boundary layer. Fig.12 displays the stability bounds of the zigzag scheme inside the reversed flow area in correspondence with the central difference scheme of Fig.6. The influence region is now twice as large as that of the central scheme. The zigzag scheme requires therefore less time steps to fulfill the CFL condition but it is not unconditionally stable either.

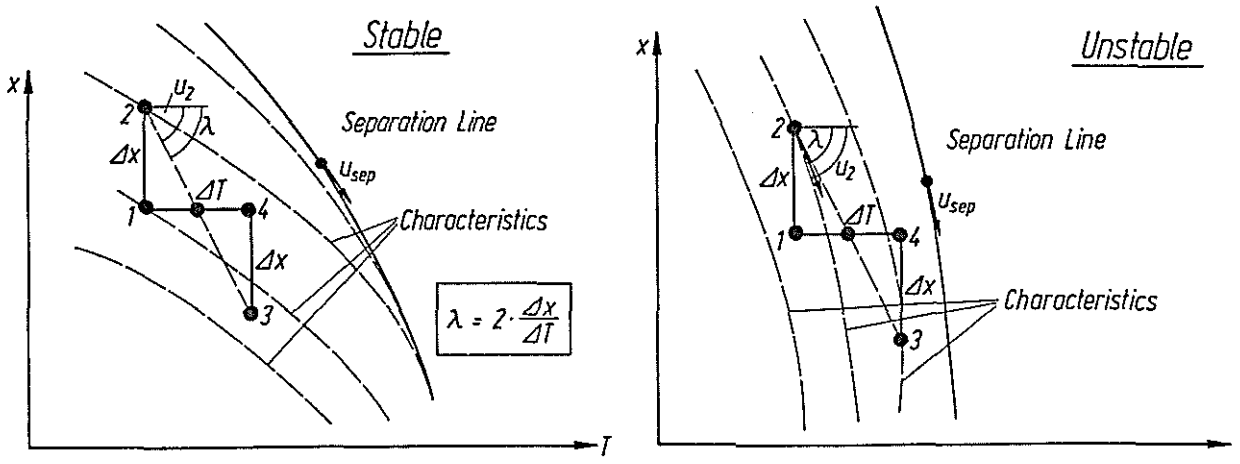

Fig.12 Stability bounds of zigzag difference scheme

4.2 Coupling with the Inviscid Method

The strong global coupling between the inviscid panel method and the boundary layer code is carried out iteratively: inviscid velocities $U_e(x,T)$ are first calculated for a complete cycle of oscillations. This velocity distribution is then used as the outer boundary condition for the boundary layer code. Due to the inverse calculation procedure the external velocity is modified (Eqs.(11),(12)). The blowing velocities $v_B(x,T)$, Eq.(13), are then taken into account in the panel method modifying the kinematic flow condition. A new external velocity distribution is calculated now including the effect of boundary layer displacement. A second global cycle is then started, etc.

4.3 Results

Fig.13 shows vectors of the maximum reversed flow velocities (upper plots) and integral curves of these vector fields (lower plots) again for two different amplitudes of oscillations and $\alpha_0 = 15°$ mean incidence. These plots correspond to Fig.9 with

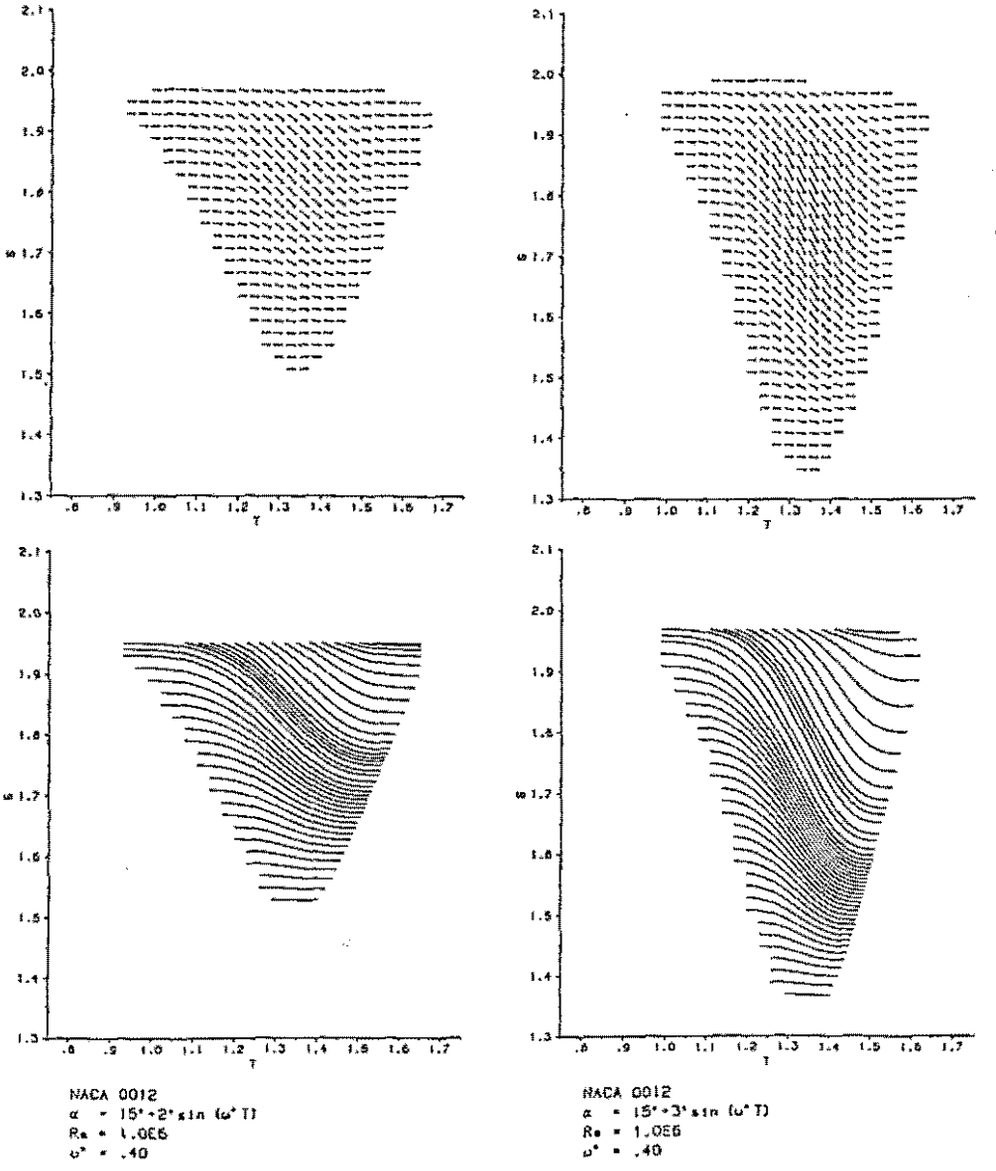

Fig.13 Maximum reversed velocity vectors and integral curves (inverse mode)

results from the boundary layer calculation in the direct mode. In the inverse case, the limiting process of forming envelopes of the integral curves is avoided. The external velocities are now allowed to adjust to the development of the boundary layer displacement effect.

Fig.14 presents integral curves of the velocity vectors inside the boundary layer and along the profile upper surface for three different incidences during the oscillatory cycle. These curves are not to be interpreted as streamlines. They are integrated from the instantaneous velocity (u,v) distributions inside the boundary layer. In Fig.14 only a very narrow region close to the wall is displayed:

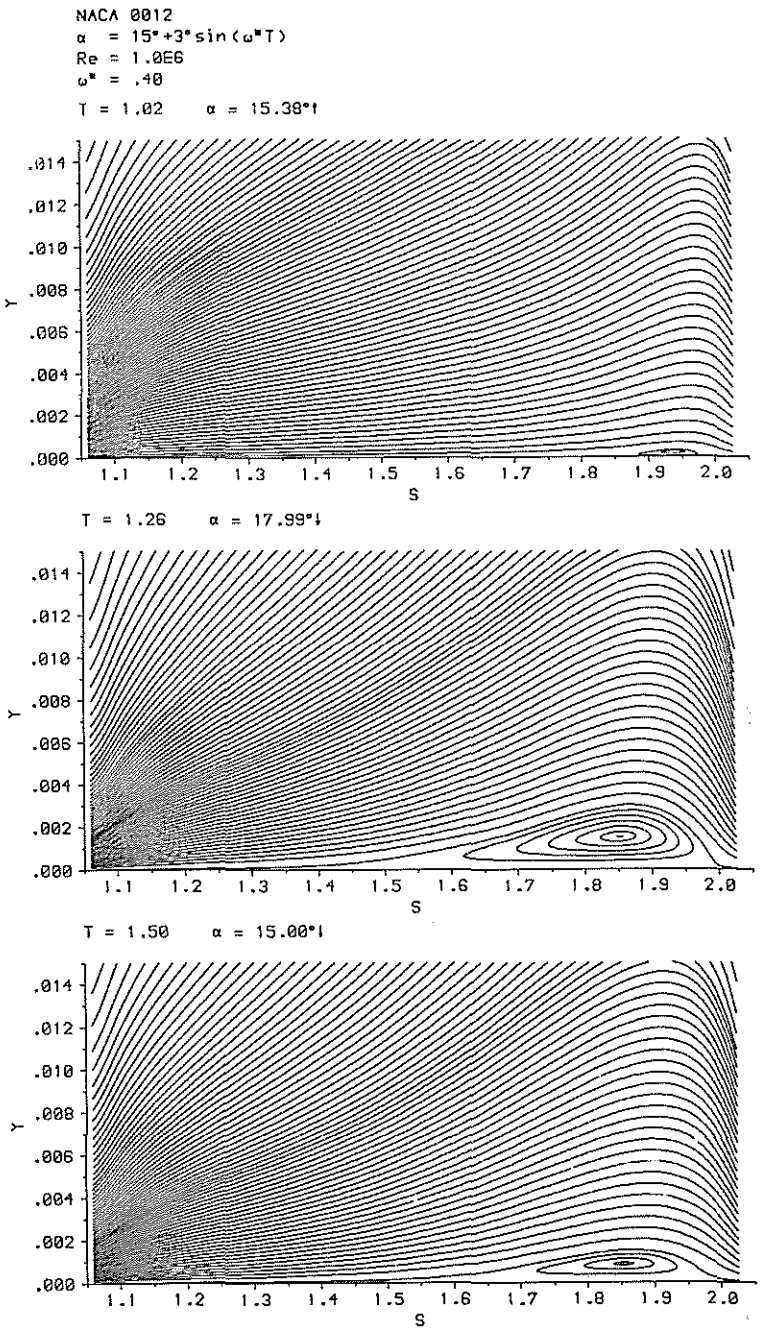

Fig.14 Recirculation areas inside the boundary layer

At about $\alpha = 15°$ upstroke (top diagram) a recirculation area develops near the trailing edge which rapidly increases in size up to the maximum incidence of $\alpha = 18°$ (middle plot). Beyond the maximum incidence the recirculation area still has a large spatial extension down to $\alpha = 15°$ (bottom plot) due to hysteresis effects. The plots show further that the integral curves are bent along the recirculation zone and compressed toward the trailing edge. The recirculation zone stays completely on the airfoil. Experimental investigations have shown, however, that the recirculation area is extended beyond the trailing edge. This deficiency of the numerical method is mainly due to the neglection of the wake displacement which is a sink effect on the airfoil influencing the Kutta condition. Future extension of the present method should therefore sufficiently include the wake displacement.

Finally, Fig.15 displays the calculated lift and moment curves for a moderate incidence case compared with experimental data [11]. The dotted slopes indicate the results of the inviscid panel method. The solid curves show the results including the inverse boundary layer calculation after one global cycle. For this case where no reversed flow occurs during the oscillatory cycle, the

agreement between theory and data is very good. It is assumed that correspondingly good results will be achieved at higher incidence variations if unsteady wake effects are taken into account in the coupling procedure.

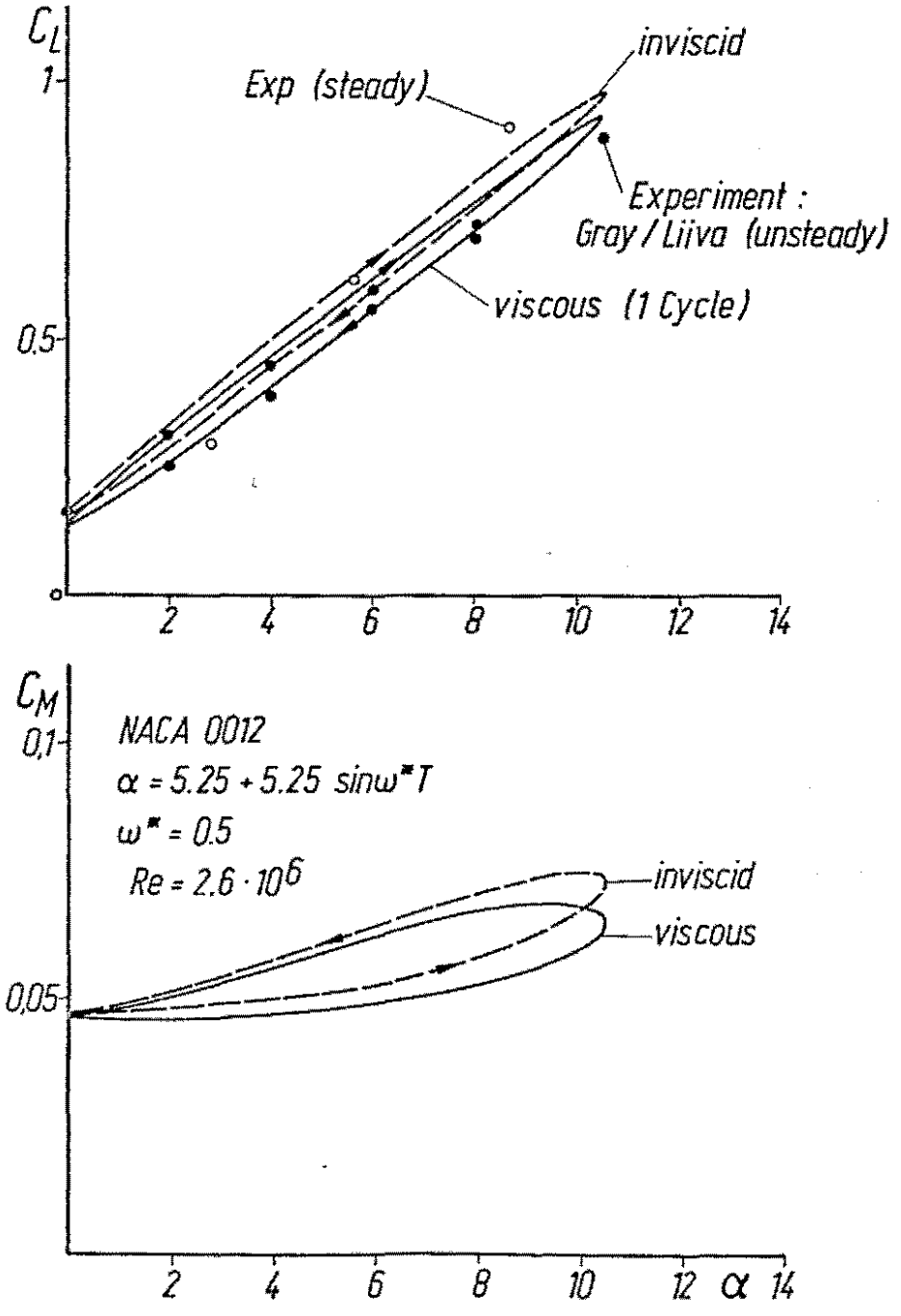

Fig.15 Unsteady lift/moment distributions: inviscid, viscous, experimental data

5. Concluding Remarks

For the investigation of unsteady viscous/inviscid interaction phenomena coupling procedures between a panel method and unsteady boundary layer codes have been developed. Working in the direct mode where the outer inviscid velocity distribution is unchanged, it has been shown that the calculation can be extended into regions of reversed flow. The asymptotic behavior of boundary layer quantities within the reversed flow area signals unsteady separation. By investigation of the maximum reversed flow velocities it has been shown that the corresponding integral curves form envelopes which are interpreted as the locations of unsteady separation. The information on separation locations and separation velocities may serve as inputs for a modified panel method.

Working in the inverse mode, the external velocity distribution is adjusted to the development of the boundary layer displacement thickness. Analogous integral curves of the maximum reversed flow velocities do not show the asymptotic behavior of the direct mode. A singularity in the boundary layer solution is obviously avoided in the inverse mode. For moderate incidence variations the lift and moment curves agree well with experimental data. For higher incidences the effect of the wake has a severe influence on the results. Modification of the method to consider the boundary layer along the unsteady wake as well as a representation of the wake displacement by a sink distribution in the panel method will be necessary future activities.

6. References

1. L.W. Carr, W.J. McCroskey, K.W. McAlister, S.L. Pucci, D. Lambert — An Experimental Study of Dynamic Stall on Advanced Airfoil Sections. NASA TM 84245 (1984); also: USA AVRADCOM TR 82-A-8 (1982).

2. L.W. Carr, K.W. McAlister, W.J. McCroskey — Analysis of the Development of Dynamic Stall Based on Oscillating Airfoil Experiments. NASA TN D-8382 (Jan. 1977).

3. T. Cebeci, L.W. Carr — Computation of Unsteady Turbulent Boundary Layers with Flow Reversal and Evaluation of Two Separate Turbulence Models. NASA TM 81259 (1981).

4. W. Geißler — Unsteady Boundary-Layer Separation on Airfoils Performing Large Amplitude Oscillations — Dynamic Stall. In: "Unsteady Aerodynamics — Fundamentals and Applications to Aircraft Dynamics," AGARD CP No.386, 6-9 May 1985, Göttingen, W. Germany.

5. W. Geißler — Unsteady Laminar Boundary Layer Calculations on Oscillating Configurations Including Backflow. NASA TM 84219 (1983).

6. W. Geißler — Calculation of Unsteady Airloads on Oscillating Profiles by a Time-Marching Procedure. DFVLR Internal Report IB 232-84J05 (1984).

7. T. Cebeci, A.M.O. Smith — Analysis of Turbulent Boundary Layers. New York: Academic Press, 1974.

8. W. Geißler — Three-Dimensional Laminar Boundary Layer over a Body of Revolution at Incidence and with Separation. AIAA J. Vol.12, No.12 (1974) pp.1743-1745.

9. W.R. Sears — Unsteady Motion of Airfoils with Boundary-Layer Separation. AIAA J., Vo.14, No.6 (1979) pp.216-220.

10. T. Cebeci, R.W. Clark — An Interactive Approach to Subsonic Flows with Separation. In: "Proc. 2nd Symposium on Numerical and Physical Aspects of Aerodynamic Flows," 17-20 Jan. 1983, Cal. State Univ. Long Beach, Session 5, Paper 2.

11. L. Gray, I. Liiva — Two-Dimensional Tests of Airfoils Oscillating Near Stall. Volume II: Data Report. USAAVLABS Rpt. 68-13B (1968).